Accurate Estimation of Inter-channel Stimulated Raman Scattering in C+L+U Ultra-wideband WDM Systems beyond Raman Shift Frequency

Kosuke Kimura
NTT Network Innovation Laboratories
NTT Corporation
1-1 Hikarinooka, Yokosuka,
Kanagawa, Japan
kousuke.kimura@ntt.com

Shimpei Shimizu
NTT Network Innovation Laboratories
NTT Corporation
1-1 Hikarinooka, Yokosuka,
Kanagawa, Japan
shimpei.shimizu.ge@hco.ntt.co.jp

Takayuki Kobayasi
NTT Network Innovation Laboratories
NTT Corporatin
1-1 Hikarinooka, Yokosuka,
Kanagawa, Japan
takayuki.kobayashi.wt@hco.ntt.co.jp

Takushi Kazama
NTT Device Technology Laboratories
NTT Corporation
3-1 Morinosato Wakamiya, Atsugi,
Kanagawa, Japan
takushi.kazama.me@hco.ntt.co.jp

Koji Enbutsu
NTT Device Technology Laboratories
NTT Corporation
3-1 Morinosato Wakamiya, Atsugi,
Kanagawa, Japan
koji.enbutsu.cm@hco.ntt.co.jp

Takeshi Umeki
NTT Device Technology Laboratories
NTT Corporation
3-1 Morinosato Wakamiya, Atsugi,
Kanagawa, Japan
takeshi.umeki.zv@hco.ntt.co.jp

Yutaka Miyamoto
NTT Network Innovation Laboratories
NTT Corporation
1-1 Hikarinooka, Yokosuka,
Kanagawa, Japan
yutaka.miyamoto.fb@hco.ntt.co.jp

***Abstract*—The U-band is a promising candidate for an additional band used in ultra-wideband (UWB) WDM systems besides the S+C+L-band as the U-band has lower fiber attenuation and fiber nonlinear coefficients than the E-band. In ultra-wideband (UWB) WDM systems, inter-channel stimulated Raman scattering (ISRS) must be taken into account. We experimentally measured and numerically calculated ISRS in C+L+U-band systems with bandwidth beyond the Raman shift frequency for maximum Raman gain. Our results demonstrate that in the C+L+U-band systems, accurate ISRS estimations require an accurate Raman gain coefficient (RGC) spectrum instead of the triangular approximation of the RGC, which causes ISRS estimation error on both sides of the spectrum.**

Keywords—inter-channel stimulated Raman scattering, ultra-wideband WDM systems, optical transmission modeling

I. INTRODUCTION

The demand for ever-increasing data traffic and cost-efficient traffic upgrades have encouraged the exploration of ultra-wideband (UWB) wavelength division multiplexing (WDM) transmission technologies [1]–[7], which can utilize already deployed fibers. Transmission in the S+C+L-band has been investigated [1], [2], [4], [6]. Moreover, the use of the U-band has been considered [8], [9]. The advantages of using the U-band are lower fiber attenuation and larger effective areas than the E-band [10]. The larger effective areas in the U-band will reduce fiber nonlinearity. Conventional problems in the U-band, such as optical signal generation and optical amplification, are studied by using periodically poled $LiNbO_3$ (PPLN)-based optical parametric amplifiers (OPAs) [2], improving the feasibility of using the U-band.

In UWB WDM systems, inter-channel stimulated Raman scattering (ISRS) [11] must be taken into account as ISRS causes signal power to transfer from shorter wavelengths to longer wavelengths. To estimate the transmission performance of UWB WDM systems quickly and accurately, closed-form Gaussian noise (GN) models that take ISRS into consideration have been proposed [12]–[18]. These closed-form GN models enable fast estimation of non-linear interference (NLI). In [12], [13], to avoid excessive errors, the NLI estimation procedure involves numerically solving the coupled equations (CEs) [19] and then finding the exact power profile of every WDM channel affected by ISRS. A factor that affects the calculation result of ISRS is the approximation of the Raman gain coefficients (RGCs) of fiber transmission lines. For conventional systems within the C+L-band (~11 THz), the RGCs can be approximated as a triangle [20]. Triangular approximation (TA) assumes that the RGCs increases linearly until a Raman shift frequency (~14 THz) but ignores the RGCs above the Raman shift frequency. For UWB systems with a bandwidth beyond the Raman shift frequency, the RGCs cannot be accurately approximated by TA [17]. Thus, using an accurate RGC spectrum instead of TA has been proposed for UWB WDM systems [12]. However, ISRS estimation errors caused by TA in UWB WDM systems remain unclear. Moreover, while ISRS in the S+C+L-band has been experimentally investigated, ISRS in UWB WDM systems containing the U-band has yet to be studied.

In this study, we experimentally measured ISRS in the C+L+U band (~16 THz) and then compared the ISRS with two kinds of ISRS numerically calculated by using TA or an accurate RGC spectrum. The accurate spectrum is obtained by interpolating an RGC spectrum shown in [21]. These comparisons used 40-km standard single-mode fiber (SSMF) or non-zero dispersion-shifted fiber (NZ-DSF) as a transmission line. These comparisons demonstrate that TA causes ISRS estimation errors on both sides of the spectrum and an accurate RGC spectrum is required for accurate ISRS estimations in C+L+U-band WDM systems.

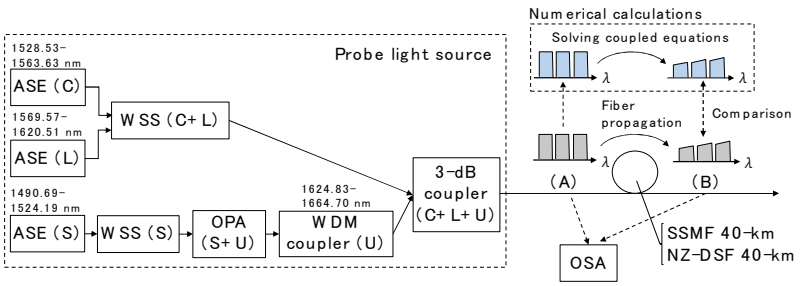

Fig. 1 Experimental setup for measuring optical spectra in C+L+U-band affected by ISRS.

II. METHODS

We begin with an explanation of the experimental measurements and then the numerical calculations. The results of the experimental measurements and the numerical calculations were compared.

A. Experimental measurements

Figure 1 shows our experimental setup for measuring optical spectra in the C+L+U-band affected by ISRS. The probe light in the C+L+U-band was generated in the dashed line box. Here, amplified spontaneous emission (ASE) in the C- and L-band were multiplexed with a wavelength selective switch (WSS), where their spectra were simultaneously flattened. ASE in the U-band was generated by using wavelength conversion with a periodically poled $LiNbO_3$ (PPLN)-based optical parametric amplifier (OPA) from ASE in the S-band as in [9]. ASE in the S-band was equalized with a WSS so that the spectrum was flattened after the wavelength is converted by the OPA. The output of the OPA contains the converted ASE in the U-band and the original S-band component. The original S-band component was removed by a WDM coupler. The ASE in the C+L-bands and in the U-band were multiplexed with a 3-dB coupler. The wavelength (frequency) ranges of the probe light were 1528.53–1563.63 nm (191.73–196.13 THz) in the C-band, 1569.57–1620.51 nm (184.00–191.00 THz) in the L-band, and 1624.83–1664.70 nm (180.09–184.51THz) in the U-band. The input powers to the transmission line were 19.2 dBm in the C-band, 16.8 dBm in the L-band, and 15.4 dBm in the U-band; the total input power was 22.2 dBm, which was the maximum power yielded by the setup. The transmission line was 40 km of either SSMF or NZ-DSF. Before and after transmission, the optical spectra of the probe light were measured with an optical spectrum analyzer (OSA). Figure 2 shows the optical spectra before transmission. The red line corresponds to a spectrum experimentally measured with a 100-GHz resolution at point (A) in Fig. 1. The blue line corresponds to a spectrum used in the numerical calculations which will be explained in the following section. The sampling frequency interval of the blue spectrum changed from that of the red spectrum (22.5 GHz) to 100 GHz.

B. Numerical calculations

The ISRS for a WDM signal propagating in an optical fiber transmission line, which contains N channels, can be expressed by CEs [19]:

$$\begin{cases} \dfrac{\partial P_1}{\partial z} = \displaystyle\sum_{j=2}^{N} C_R(f_1, f_j) P_j P_1 - \alpha(f_1) P_1 \\ \dfrac{\partial P_i}{\partial z} = \displaystyle\sum_{j=1}^{i-1} C_R(f_i, f_j) P_j P_i - \sum_{j=i+1}^{N} \frac{f_i}{f_j} C_R(f_j, f_i) P_j P_i - \alpha(f_i) P_i \\ \qquad (2 \le i \le N-1) \\ \dfrac{\partial P_N}{\partial z} = -\displaystyle\sum_{j=1}^{N-1} \frac{f_N}{f_j} C_R(f_j, f_N) P_j P_N - \alpha(f_N) P_N \end{cases} \tag{1}$$

where P_i is the i-th WDM channel power, f_i is the center frequency of the i-th WDM channel, $C_R(f_s, f_p)$ is an RGC for a signal channel at f_s and a pump channel at f_p, and $\alpha(f_i)$ is a power attenuation coefficient. We calculated the ISRS using the CEs for the optical spectrum before transmission as shown in Fig. 2 and compared the numerical results with the experimental results after transmission.

Next, we use two fiber characteristics, RGCs and power attenuation coefficients, to solve the CEs. Figure 3 shows the

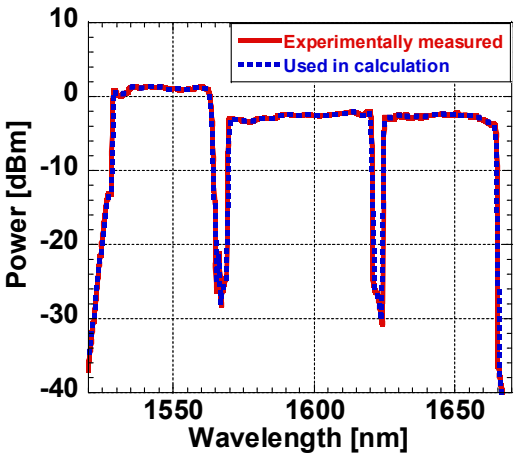

Fig. 2 Optical spectra of probe light before transmission.

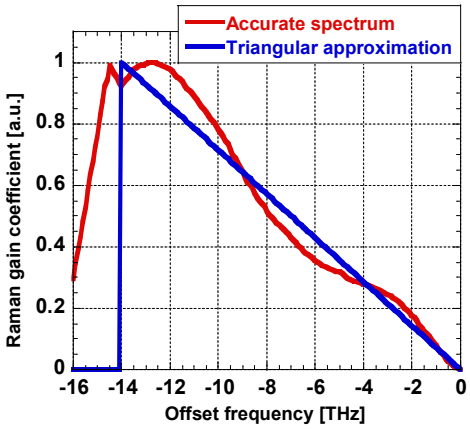

Fig. 3 Normalized Raman gain coefficient spectrum.

RGCs. The horizontal axis represents the offset frequency from a pump channel to a signal channel, and the vertical axis represents the normalized value of RGC spectra. The red line is an accurate RGC spectrum obtained from [21]. The blue line is the TA that increases linearly until an offset frequency of −14 THz [16]. Fig.3 represents the maximum range of RGC spectra used in the calculation, i.e., until an offset frequency of −16 THz. The major difference between these RGC spectra is that although the accurate RGC spectrum has finite values from −14 THz to −16 THz, the TA is 0 within the range. The peak values of the RGCs for the 1480-nm pump channel were set to 0.39 $W^{-1}km^{-1}$ for the SSMF and 0.66 $W^{-1}km^{-1}$ for the NZ-DSF [22]. Frequency dependence of the RGCs was considered by [23]:

$$C_R(f_s, f_p) = C_R(f_s^{ref}, f_p^{ref}) \frac{f_s}{f_s^{ref}} \frac{A_{eff}(f_s^{ref}) + A_{eff}(f_p^{ref})}{A_{eff}(f_s) + A_{eff}(f_p)} \quad (2)$$

where f_s^{ref} and f_p^{ref} are the center frequency of the reference signal and pump channels, and $A_{eff}(f)$ is an effective area. Effective areas for the SSMF and NZ-DSF across the C+L+U-band were calculated as in [10], [12].

Figure 4 shows attenuation profiles of the transmission lines. The red and blue lines correspond to the SSMF and NZ-DSF. These profiles were measured by using an optical loss analyzer for less than 1640 nm and by measuring the attenuation of the probe light in the U-band for 1640 nm or more. To avoid ISRS within the U-band, the total input power of the probe light was limited to −5 dBm.

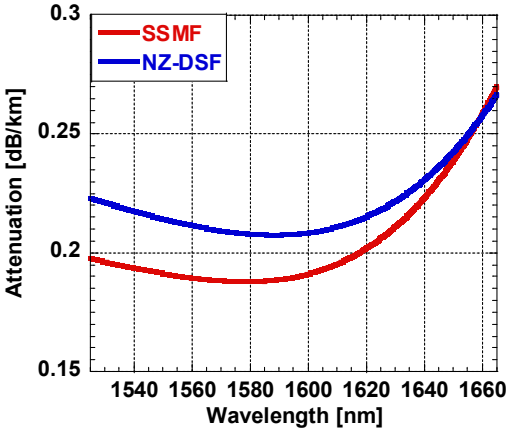

Fig. 4 Attenuation profiles of SSMF and NZ-DSF.

III. Results and Discussion

Figure 5 (a) and (b) show the optical spectra of the probe light after the 40-km SSMF and NZ-DSF transmission. These spectra in Fig. 5 are enlarged around the top. The red, blue, and green lines represent the experimental result, the numerical result with the TA, and the numerical result with

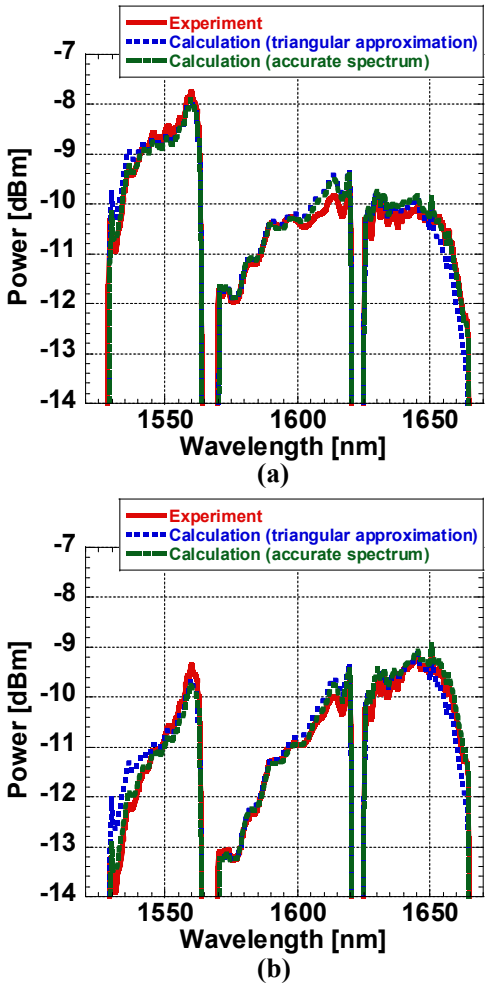

Fig. 5 Optical spectra of probe light after (a) SSMF and (b) NZ-DSF transmission.

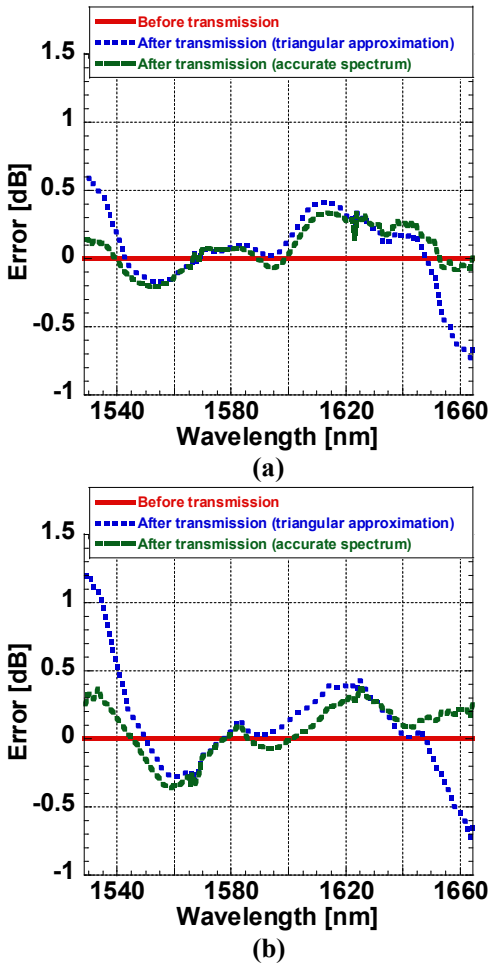

Fig. 6 Errors calculated by subtracting experimental result from numerical results. (a) SSMF, (b) NZ-DSF.

the accurate RGC spectrum, respectively. The experimental result was measured at point (B) in Fig. 1. The spectra after NZ-DSF transmission tilted compared to the spectra after the SSMF transmission due to the larger RGC and attenuation of the NZ-DSF. The calculation results are almost the same in the middle but differ on both sides of the spectra. To examine the accuracy of the calculated ISRS in more detail, we calculated the errors by subtracting the experimental result from the numerical results in dB. Figures 6 (a) and (b) show the errors for the SSMF and NZ-DSF. The red line corresponds to the errors before the transmission shown in Fig. 2 and is 0 dB across the C+L+U-band. The blue and green lines correspond to the errors after the transmission for the TA and accurate RGC spectrum. The errors for the accurate RGC spectrum were comparatively flat for both the SSMF and NZ-DSF. In contrast, the errors for TA increased on both sides and were positive at shorter wavelengths and negative at longer wavelengths. The maximum absolute error was 0.7 dB for the SSMF and 1.2 dB for the NZ-DSF. These results demonstrate that the accurate RGC spectrum enables accurate estimations of ISRS across the C+L+U-band. These results also indicate that the TA underestimates ISRS loss at shorter wavelengths and ISRS gain at longer wavelengths and this ISRS underestimation increases with RGCs. The underestimation of ISRS can obstruct accurate modeling of UWB WDM systems that have bandwidth beyond the Raman shift frequency for maximum Raman gain. Thus, an accurate RGC spectrum should be required for accurate ISRS estimations in UWB WDM systems.

IV. Conclusion

We experimentally measured and numerically calculated ISRS in C+L+U-band WDM systems. Our results demonstrate that TA causes ISRS estimation errors on both sides of the spectrum and an accurate RGC spectrum is required to estimate the ISRS accurately in C+L+U-band WDM systems. Our results provide insights into the accurate modeling of UWB WDM systems above the C+L-band.

References

[1] F. Hamaoka, K. Saito, A. Masuda, H. Taniguchi, T. Sasai, M. Nakamura, T. Kobayashi, and Y. Kisaka, "112.8-Tb/s real-time transmission over 101 km in 16.95-THz triple-band (S, C, and L Bands) WDM configuration, " OECC/PSC2022, PDP-A-3.

[2] T. Kobayashi, S. Shimizu, M. Nakamura, T. Umeki, T. Kazama, R. Kasahara, F. Hamaoka, M. Nagatani, H. Yamazaki, H. Nosaka, and Y. Miyamoto, "Wide-band inline-amplified WDM transmission using PPLN-based optical parametric amplifier," J. Lightw. Technol., vol. 39, no. 3, pp. 787–794, 2021.

[3] T. Kato, H. Muranaka, Y. Tanaka, Y. Akiyama, T. Hoshida, S. Shimizu, T. Kobayashi, T. Kazama, T. Umeki, K. Watanabe, and Y. Miyamoto, "WDM transmission in S-band using PPLN-based wavelength converters and 400-Gb/s C-band real-time transceivers," OECC/PSC2022, WA-3-4.

[4] B. J. Puttnam, R. S. Luís, G. Rademacher, Y. Awaji, and H. Furukawa, "Investigation of long-haul S-, C- + L-band transmission," OFC2022, W3C.5.

[5] S. Okamoto, K. Minoguchi, K. Horikoshi, A. Matsushita, M. Nakamura, E. Yamazaki, and Y. Kisaka, "A study on the effect of ultra-wide band WDM on optical transmission systems," J. Lightw. Technol., vol. 38, no. 5, pp. 1061-1070, 2020.

[6] A. Arnould, A. Ghazisaeidi, D. Le Gac, P. Brindel, M. Makhsiyan, K. Mekhazni, F. Blache, N. Fontaine, D. Neilson, R. Ryf, H. Chen, M. Achouche, and J. Renaudier, "103 nm ultra-wideband hybrid raman/SOA transmission over 3 × 100 km SSMF," J. Lightw. Technol., vol. 38, pp. 504–508, Jan. 2020.

[7] R. Emmerich, M. Sena, R. Elschner, C. Schmidt-Langhorst, I. Sackey, C. Schubert, and R. Freund, "Enabling S-C-L-band systems with standard C-band modulator and coherent receiver using nonlinear predistortion," J. Lightw. Technol., vol. 40, pp. 1360–1368, Mar. 2022.

[8] T. Kato, H. Irie, H. Muranaka, Y. Tanaka, Y. Akiyama, and T. Hoshida, "U-band transmission of real-time 200-Gb/s signal co-propagating with C+L-band WDM signal," OFC2023, Th3F.6.

[9] S. Shimizu, T. Kobayashi, A. Kawai, T. Kazama, M. Nakamura, K. Enbututsu, T. Kashiwazaki, M. Abe, T. Umeki, Y. Miyamoto, T. Kato, Y. Tanaka, and T. Hoshida, "38.4-Tbps inline-amplified transmission using PPLN-based optical parametric amplifier over 6 THz within L- and U-bands," OFC2023, Th3F.3.

[10] N. A. Shevchenko, S. Nallaperuma, and S. J. Savory, "Maximizing the information throughput of ultra-wideband fiber-optic communication systems," Opt. Express 30, 19320-19331 (2022).

[11] J. Bromage, "Raman amplification for fiber communications systems," J. Lightw. Technol., vol. 22, no. 1, pp. 79-93, Jan. 2004, doi: 10.1109/JLT.2003.822828.

[12] P. Poggiolini, "Closed form expressions of the nonlinear interference for UWB systems," ECOC2022, Tu1D.1.

[13] M. Ranjbarzefreh and P. Poggiolini, "A real-time closed-form model for nonlinearity modeling in ultra-wide-band optical fiber links accounting for snter-channel stimulated Raman scattering and co-propagating Raman amplification," arXiv:2006.03088 [eess.SP], June 2020.

[14] M. Ranjbar Zefreh, F. Forghieri, S. Piciaccia, and P. Poggiolini, "Accurate closed-form real-time EGN model formula leveraging achine-learning over 8500 rhoroughly randomized full C-band systems," J. Lightw. Technol., vol. 38, no. 18, pp. 4987-4999, 2020.

[15] D. Semrau, "Modeling of Fiber Nonlinearity in Wideband Transmission," OFC2022.

[16] D. Semrau, R. I. Killey, and P. Bayvel, "A closed-form approximation of the Gaussian noise model in the presence of inter-channel Stimulated Raman scattering," J. Lightw. Technol., vol. 37, no. 9, pp. 1924-1936, 2019.

[17] D. Semrau, L. Galdino, E. Sillekens, D. Lavery, R. I. Killey, and P. Bayvel, "Modulation format dependent, closed-form formula for estimating nonlinear interference in S+C+L band systems," ECOC2019, W.1.D.1.

[18] C. Lasagni, P. Serena, A. Bononi and J. -C. Antona, "Generalized Raman scattering model and its application to closed-form GN model expressions beyond the C+L band," ECOC2022, Tu1D.2.

[19] S. Tariq and J. C. Palais, "A computer model of non-dispersion-limited stimulated Raman scattering in optical fiber multiple-channel communications," J. Lightw. Technol., vol. 11, no. 12, pp. 1914-1924, 1993.

[20] A. R. Chraplyvy, "Optical power limits in multichannel wavelength division-multiplexed systems due to stimulated Raman scattering," Electron. Lett., vol. 20, pp. 58-59, 1984.

[21] R. H. Stolen, "Nonlinearity in fiber transmission," Proc. IEEE, vol. 68, no. 10, pp. 1232-1236, 1980.

[22] E. Pincemin, D. Grot, L. Bathany, S. Gosselin, M. Joindot, S. Bordais, Y. Jaouen, and J. Delavaux, "Raman gain efficiencies of modern terrestrial transmission fibers in S-, C- and L-band," Nonlinear Guided Waves Appl., 2002, NLTuC2.

[23] K. Rottwitt, J. Bromage, A. J. Stentz, Lufeng Leng, M. E. Lines, and H. Smith, "Scaling of the Raman gain coefficient: applications to germanosilicate fibers," J. Lightw. Technol., vol. 21, no. 7, pp. 1652-1662, 2003.